

Simulation and modeling of gallium nitride high-electron mobility transistors for non-alloyed ohmic contacts

Tung Kok Siong^a, Mohamed Fauzi Packeer Mohamed^{a*}, Siti Fatimah Abd Rahman^{a*}, Mohd Syamsul^b, Ahmad Shuhaimi Abu Bakar^c, and Alhan Farhanah Abd Rahim^d

^aSchool of Electrical and Electronic Engineering, Engineering Campus, Universiti Sains Malaysia, 14300 Nibong Tebal, Pulau Pinang, Malaysia

^bInstitute of Nano Optoelectronics Research and Technology (INOR), Universiti Sains Malaysia, 11900 Bayan Lepas, Pulau Pinang, Malaysia

^cLow Dimensional Material Research Center (LDMRC), Physics Department, Faculty of Science, Universiti Malaya, 50603 Kuala Lumpur, Malaysia

^dElectrical Engineering Studies, College of Engineering, Universiti Teknologi MARA, Cawangan Pulau Pinang, 13500 Permatang Pauh, Pulau Pinang, Malaysia

*Corresponding author. e-mail: fauzi.packbeer@usm.my (M.F.P.M) and fatimahrahman@usm.my (S.F.A.R)

Received 3 July 2024, Revised 23 September 2024, Accepted 16 October 2024

ABSTRACT

The advantages of gallium nitride (GaN) high-electron mobility transistors, such as concentrated channel electron density, superior electron mobility, and high breakdown voltage, present an opportunity to replace silicon-based devices from modern power conversion systems in the near future. The development of low-resistance ohmic contacts in aluminium gallium nitride (AlGaIn)-based GaN devices is crucial for predicting their performance. However, only limited studies have employed technology computer-aided design (TCAD) software to investigate contact resistance in GaN devices and to develop strategies for minimizing contact resistivity. Furthermore, the ohmic contact is able to be achieved only based on different configurations of metal stacks with annealing. This study, using Silvaco TCAD Atlas, first modeled contact resistance in a vertical structure and later extended the study to a lateral structure, which is more feasible for physical manufacturing. The investigation focused on various n^{++} regions with different doping levels beneath the metal to determine the best optimization for ohmic contact. The result revealed that reducing contact resistivity saturated ($1 \times 10^{-6} \Omega/\text{cm}^2$) at a thickness of 18 nm for the heavily doped layer ($\geq 1 \times 10^{19} \text{cm}^{-3}$), beyond which no significant decrease in contact resistivity was observed for varying doping levels in n^{++} layers. This study demonstrates that including a heavily doped layer between the contact and semiconductor surfaces results in the ohmic behaviour emergence in metal contacts.

Keywords: Gallium Nitride (GaN), High Electron Mobility Transistors (HEMT), TCAD simulation, Semiconductor devices, Non-alloyed Ohmic contact

1. INTRODUCTION

The invention of III-nitride wide bandgap semiconductors has been the focus of research in recent years, most extensively on gallium nitride (GaN), the representable material of third-generation semiconductors. The GaN high-electron mobility transistors (HEMT) power device is now undergoing extensive research and development. It reveals outstanding performance in high-density power devices compared to metal oxide semiconductor (MOS), bipolar junction transistor (BJT), and gallium arsenide (GaAs) devices.

GaN-based semiconductors possess unique material properties. This contender is highly suitable for high-power use due to its large bandgap (3.4 eV), great critical field (3.3 MV/cm) [1], great electron saturation speed ($3 \times 10^7 \text{cm/s}$) [2], and great operation switching recurrence [3]. GaN and its related ternary alloys $\text{Al}_x\text{Ga}_{1-x}\text{N}$ are the candidates that carry the most opportunity to take over the silicon (Si)-based devices for the future of modern power devices [4,5].

Low resistance ohmic contacts of aluminum gallium nitride (AlGaIn)/GaN-based devices are essential to achieve its forecasted device performance. In this context, the reduced ohmic resistance of the contact results in diminished power consumption, signifying enhanced power transmission efficiency [6]. However, there has been insufficient work done on the software-based technology computer-aided design (TCAD) in Silvaco Atlas of the device to study the contact resistance and manufacturing procedures to lower the contact resistivity.

Silicon material has hit its limit in scaling dimensions and enhancing performance. GaN has been discovered to offer improved performance, such as higher operating temperature, smaller dimensions, faster operation, and better efficiency than Si-based semiconductor [3,7–10]. Metal contacts are vital for semiconductors as the device needs to connect to the external world to serve its function. The metal-semiconductor interface interaction characteristic is measured using ohmic contact resistance, which must be ignorable with respect to the semiconductor surface. The contact is supposed to have a linear current-

voltage (ohmic contact) characteristic and minimal contact resistance to prevent output disruption of semiconductor devices; this is particularly obvious to modern power conversion devices, and it requires effective thermal dissipation [11–15]. Thus far, ohmic contact is only able to be achieved through different configurations of stacks of metal contact, and after being subjected to annealing, thus a new approach of heavily doped layer underneath the metal contact is studied to create the ohmic contact. Table 1 shows the parameters obtained for different methods.

Table 1. Comparison of ρ_c values and different metal schemes.

Metal Stack	Barrier layer	Annealing T (°C)	Contact Resistivity, ($\rho_c \Omega\text{-cm}^2$)	Ref.
Ti/Al/ γ /Au (where γ = Ni, Mo, Ti, etc.)	n-GaN	750–850	$10^{-5} \sim 10^{-7}$	[16–20]
Al	n-GaN	600	5×10^{-6}	[21]
Ti/Al	n-GaN	900	8×10^{-6}	[22]
Ti	n-GaN	950	3×10^{-6}	[23]
Ti/Al/Cr/Mo/Au	n-GaN	875	1.1×10^{-6}	[24]

In this study, the electrical and structural aspects of n-GaN were evaluated with different n^{++} layer thickness under the contact, and their performances were analyzed. The work was carried out using Silvaco TCAD Atlas simulation software, and the results were based on non-alloy ohmic contact, i.e., without annealing [25,26]. The contact resistivity allowed us to evaluate the critical transport model between metal and GaN surfaces.

2. METHODOLOGY

All the structural aspects were simulated using Silvaco TCAD Atlas tools [27]. Groups of Atlas code must follow specific orders to avoid the program's termination. The first group covered structure specifications: the mesh, region, electrode, and doping statements. Material models' specifications consisted of the second group's materials, models, contact, and interface statements categories. Numerical method selection was in the third group. The fourth group was to provide the solution on output; these consisted of the save, solve, log, and load specifications. The last group did the result analysis by evaluating the data and visual aids by the graph; this was done by extracting Tonyplot statements. To define the Atlas structure, we first needed to determine a mesh. The program analyzed each line that crossed the point in a structure. Thus, the lines should frequently cross in the point of areas of interest and less frequently in areas where the structure was non-critical. For the structural properties involving the concentration of doping, materials, and models involved, the Atlas command language was used. Then, the electrical characteristic current-voltage (I-V) properties were extracted using the Atlas solver.

Six different vertical distances at a time were constructed for 5, 9, 13, 17, 21, and 25 μm between the metal contacts of

aluminum (Al). The simulations were performed based on a vertical device layout where the metal was placed on both sides of the semiconductor. Then, the simulation was followed by the lateral structure where the metal contacts were placed at the left and right top corners with the spacing of 5, 9, 13, 17, 21, and 25 μm between the left and right metal contact and n^{++} layer place under the metal contact with varied thickness of 2 nm/ 6 nm/ 18 nm/ 54 nm and doping concentration of $5 \times 10^{17} \text{ cm}^{-3} \sim 1 \times 10^{20} \text{ cm}^{-3}$.

The tunnelling model of Universal Schottky was selected to replicate the thermionic and field emission occurring between the metal contact and the highly doped semiconductor. Effective mass calibration was set for various doping n^{++} layers. Masetti's default mobility model was chosen for this simulation work. Then, the Transfer Length method (TLM) was applied to study the data extracted from the program's output. This approach was adapted from Sharma et al. [28]. TLM was plotted based on the total resistance (R_T) extracted against spacing (d) which was pre-defined between the contacts. The vertical device structure was built in the simulation to evaluate the properties of total resistance and metal contact spacing, and the data were analyzed. Following that, the device with the lateral structure, where the voltage on the semiconductor between the metal electrodes, was now applied. Different spacing between the contacts was achieved with different thickness on the semiconductor layer and doping concentration to gain a TLM plot. The vertical structure and its equivalent circuit model are shown in Figure 1(a).

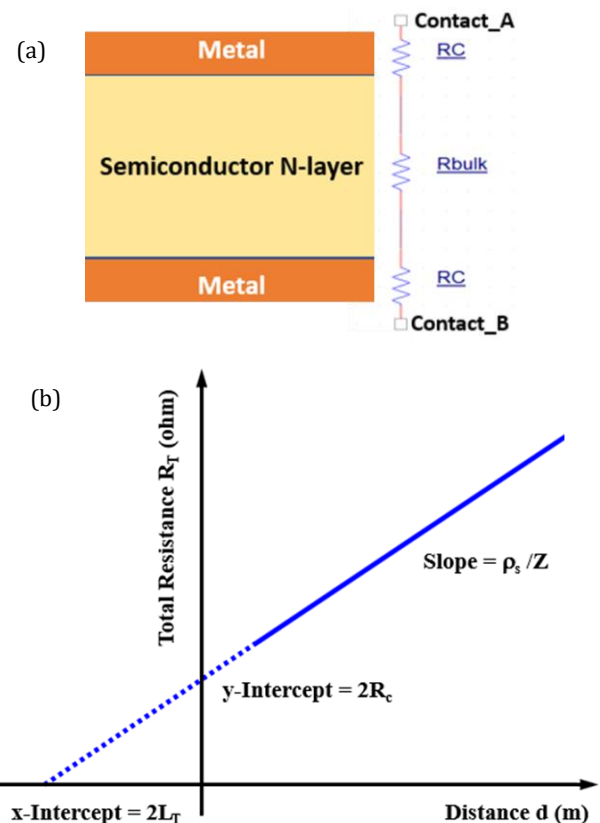


Figure 1. (a) Vertical-form of device structure with the equivalent circuit model.(b) The Transfer Length method (TLM) plot of R_T vs. d [27].

In this structure, R_c represents the contact resistance between the surface of the metal-semiconductor. R_{bulk} contributed to the resistance of the semiconductor bulk of the device. The total resistance between top contact and bottom contact can be expressed as Equation (1):

$$R_T = 2R_c + R_{bulk} \quad (1)$$

R_c represents the resistance at the junction between the metal and semiconductor, while R_{bulk} represents the resistance of the bulk of the n-GaN semiconductor. Furthermore, the semiconductor's bulk resistance in terms of sheet resistance can be written as Equation (2) [27]:

$$R_{bulk} = \rho_s * d/Z \quad (2)$$

The sheet resistance of a thin layer material is denoted as ρ_s . The distance between the metal contacts is represented by d , while Z refers to the width of the semiconductor where the current flows. Therefore, Equation (3) can be used to calculate the total resistance, R_T [27]:

$$R_T = 2R_c + (\rho_s/Z) d \quad (3)$$

Figure 1(b) illustrates that the y-intercept of the R_T vs. d plot represents double the contact resistance (R_c), whereas the gradient of the line indicates the sheet resistance of the bulk n-GaN semiconductor. TLM plot extracts the parameters based on the points approaching the linear fit of the graph. The y-intercept indicates the contact resistance, while sheet resistance is retrieved from the graph's slope, which is a unit per width. Transfer length (L_T) is a parameter that can be obtained at the x-intercept of the graph. This transfer length provides the applicable length needed where the current flows through the metal-semiconductor surface.

3. RESULTS AND DISCUSSION

3.1. Characterization of Vertical Device Structure

Figure 2(a) shows the structure of the vertical unit device of $4 \mu\text{m}$, with a thickness of $5 \mu\text{m}$ and uniformly doped at $1 \times 10^{18} \text{ cm}^{-3}$. The n-GaN bulk thickness was systematically altered to 5, 9, 13, 17, 21, and $25 \mu\text{m}$ in order to replicate the gap between the upper and lower metal contacts. As the most significant region of interest was the interface between metal and semiconductor, at the interface, a very minute mesh was defined as depicted in Figures 2(b) and (c), respectively, for the accuracy of the simulation. Accuracy required a fine mesh that could resolve all significant features of the structure solution. Fine mesh was required in this area because of the possibility of abrupt variation of electrical parameters. Moreover, finer meshes triggered the program to solve a lot more points based on the basic equations to obtain accurate simulation.

By plotting the I-V curves, the TLM pattern consisting of total resistance (R_T) vs. the gap between the metal contacts (d) was retrieved. Since the metal contacts were placed on both sides of the semiconductor for a vertical structure of GaN and the spacing, d , of the semiconductor varied (i.e., 5, 9, 13, 17, 21, and $25 \mu\text{m}$), the theory of transfer length did not stand here as current in fact flowed through the metal

contact by occupying entire cross-section. The total points of resistance for the TLM plot were calculated using these varied levels of evenly distributed spacing. Figures 3(a) and (b) depict the energy band-diagram for the vertical semiconductor with a working-function aluminum (Al) contact of $\phi_m = 4.3 \text{ eV}$, accordingly. The sample characteristic of I-V is illustrated in Figure 3(c).

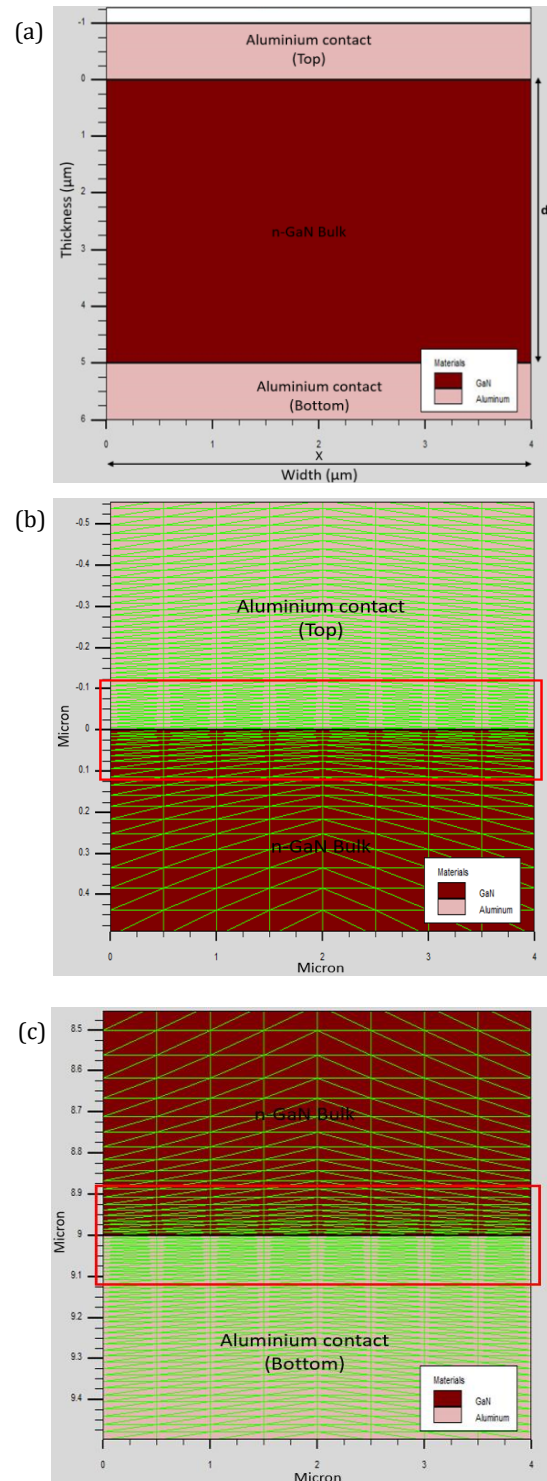


Figure 2. (a) Vertical structure of the n-GaN device with thickness of $5 \mu\text{m}$. Mesh-defined device's interface for (b) top of the structure and (c) bottom of the structure between semiconductor and metal, respectively.

For different space charge region thickness within the metal-semiconductor surface, different carrier transport mechanisms can occur at the interface, relying on the semiconductor doping level N_D , as illustrated in Figure 4. Doping density of $1 \times 10^{18} \text{ cm}^{-3}$ induced thermionic field emission between the metal contact and semiconductor. The presence of a highly doped layer between the contact surface and the semiconductor causes the creation of an ohmic contact, as seen by the depicted I-V curve. The slope became less steep when the distance was wider due to the GaN bulk acting as a resistor, and the resistor nature of resistance is inversely proportional to distance. As doping increased, the contact with metal became ohmic contact.

Note that the contact resistivity continued to decrease when the n-type GaN doping increased. As the level of semiconductor doping escalated, the probability of tunnelling also escalated, causing a shift in the flows of current from metal to semiconductor via field emissions. With an increase in doping, decreased resistance was observed. The energy of the conduction band was reduced when a layer with high doped was inserted between the metal and semiconductor layers.

A narrower tunnelling barrier caused more electrons to flow through a metal-semiconductor interface. Thus, more current flow resulted in lower contact resistance. Figure 4 shows the comparison of barrier width for doping density of $1 \times 10^{19} \text{ cm}^{-3}$ and $1 \times 10^{20} \text{ cm}^{-3}$, respectively. The heavily doped layer between the surface of metal and semiconductor would make contact become ohmic contact, as shown in the I-V curve [Figure 3(c)].

Furthermore, the TLM plotted the total resistance (R_T) vs. spacing between contact (d) obtained by retrieving various TLM points, as shown in Figure 5. It showed that the resistance increased when the value of spacing increased from 5–25 μm , and the doping parameters of $1 \times 10^{18} \text{ cm}^{-3}$ derived the mobility of $389 \text{ cm}^2/\text{V}\cdot\text{s}$. In addition, Equation 4 [29] could be used to manually calculate and verify the simulated value of sheet resistance. The parameters extracted from the TLM plot in Figure 5 are shown in Table 2. Note here that the difference between vertical structure and lateral structure is, for vertical structure, the theory of transfer length can be ignored as current flowed through the metal contact by occupying the entire cross-section, whereas for lateral structure, there is current crowding in the edge of metal contacts. In this case for vertical structure, the main purpose here was to validate the model by comparing the simulation extracted parameters versus the theoretical calculations value.

$$\rho_s = 1/(q\mu N_d) = 1/(1.6\text{E-}19 \cdot 389 \cdot 1\text{E+}18) = 0.0161 \quad (4)$$

Table 2. Parameters obtained from the Transfer Length method

Contact resistance (Ω)	Sheet resistance (Ω/square)	Sheet resistivity ($\Omega\text{-cm}$)	Calculated sheet resistivity ($\Omega\text{-cm}$)
27.6	160	0.0161	0.0160

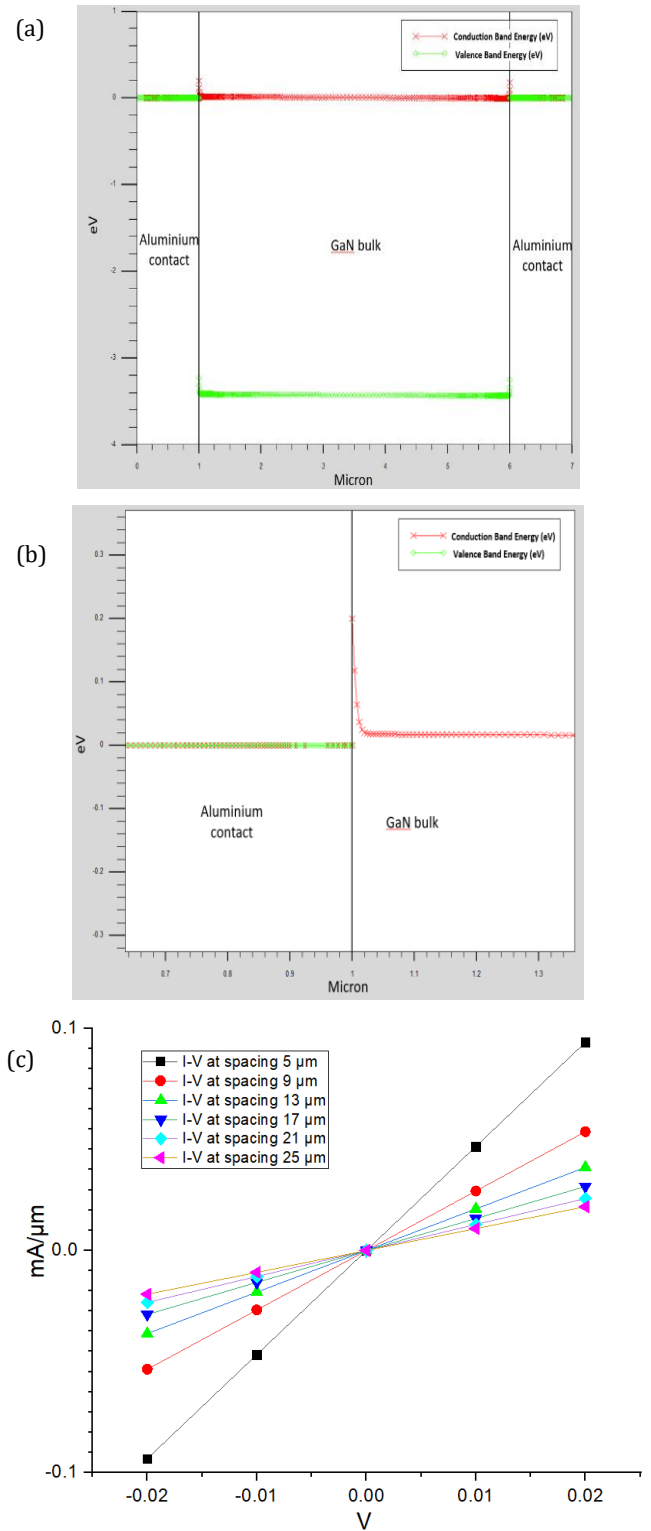


Figure 3. (a) Energy diagram for Aluminum (Al) contact and GaN bulk with metal work-function, $\phi_m = 4.3 \text{ eV}$. (b) Energy diagram for interface between Al contact and GaN bulk ($\phi_m = 4.3 \text{ eV}$). (c) Current-voltage (I-V) characteristic of $1 \times 10^{18} \text{ cm}^{-3}$ n-GaN with Al contacts.

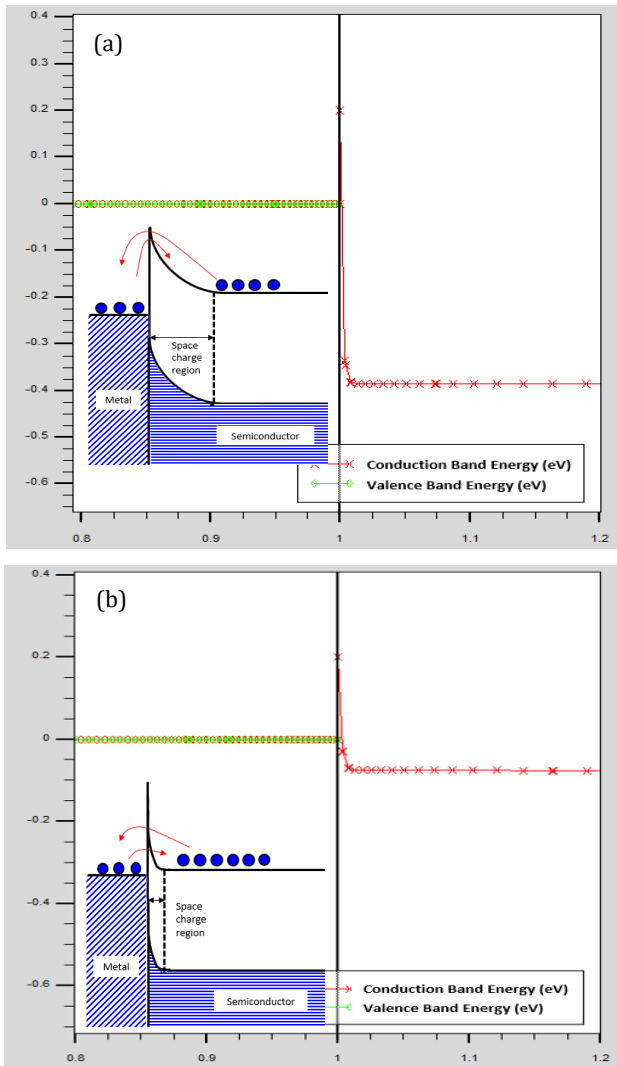


Figure 4. Barrier width for doping density of (a) $1 \times 10^{19} \text{ cm}^{-3}$ and (b) $1 \times 10^{20} \text{ cm}^{-3}$. The diagrams in the inset figures depict carrier transport mechanisms that related to N_D doping levels.

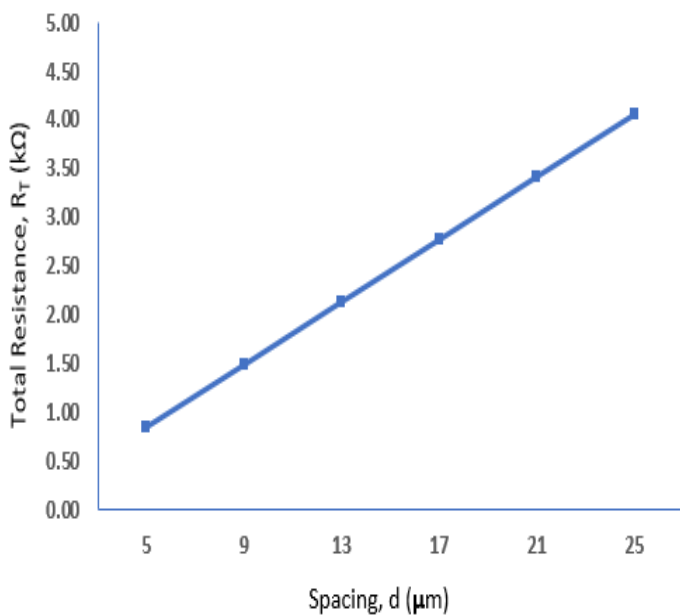


Figure 5. TLM plot for n-GaN of $1 \times 10^{18} \text{ cm}^{-3}$ with metal work-function $\phi_m = 4.3 \text{ eV}$.

3.2. Characterization of Lateral Device Structure

Apart from the vertical type of n-GaN device, the most practical device is the lateral structure type [Figure 6(a)]. The lateral structure is typically built with the metal contact placed on the right and left top of the device. Table 3 summarizes the structural dimensions of the device. To understand the characteristics of the lateral n-GaN device, a basic simulation of the said device with N-doping of $1 \times 10^{19} \text{ cm}^{-3}$ and metal work-function of $\phi_m = 4.3 \text{ eV}$ was performed. To observe the ohmic I-V characteristic, the output current was plotted against the input voltage at various spacings, as shown in Figure 6(b). As expected, linear I-V characteristics were observed because of the high doping, reducing the barrier height.

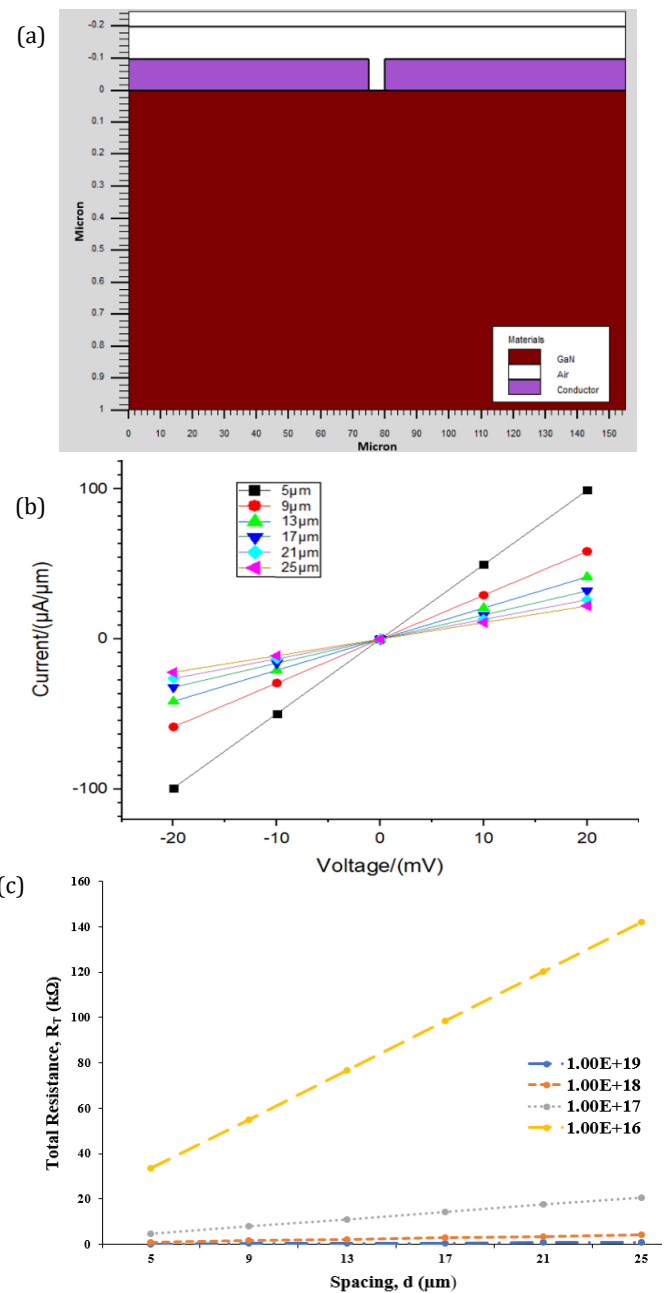


Figure 6. (a) Formation of lateral n-GaN. (b) I-V characteristics of lateral n-GaN with N-doping of $1 \times 10^{19} \text{ cm}^{-3}$ ($\phi_m=4.3 \text{ eV}$). (c) TLM plot at work-function of $\phi_m=4.3 \text{ eV}$ when n-GaN doping varied from $1 \times 10^{16} \text{ cm}^{-3}$ to $1 \times 10^{19} \text{ cm}^{-3}$.

Furthermore, the simulation of different doping conditions was shown in the form of the TLM plot [Figure 6(c)]. It is a well-established fact that there is an inverse relationship between mobility and doping concentration, as the presence of doping impurities leads to ionization at normal room temperature. An electrostatic interaction was present between the electrons or holes and the ionized impurities. This coulomb interaction produced scattering or collisions and altered the charge carrier's velocity characteristics. Thus, mobility was inversely proportional to ionized impurity concentration in the semiconductor. In the TLM plot, therefore, as the amount of n-GaN doped rose, the slope which represented the sheet resistance decreased as the slope reflected the sheet resistance. Nevertheless, the decline in mobility was significantly less pronounced to the rise in doping. As the level of semiconductor doping escalated, the sheet resistance exhibited a quick drop.

In addition, to obtain the best result of ohmic contacts between metal-semiconductor surfaces, a heavily doped layer ($1 \times 10^{19} \text{ cm}^{-3} \sim 1 \times 10^{20} \text{ cm}^{-3}$) was placed under the metal contact with n-GaN doping $1 \times 10^{17} \text{ cm}^{-3}$. The structure n^{++} layer under contact with the metal-semiconductor interface is depicted in Figure 7(a). The thickness and doping concentration of the n^{++} layer was altered in order to investigate the impact of n^{++} layer characteristics on current density. This was done by varying the thickness of the n^{++} layer at 2, 6, 18, and 54 nm. Figure 7(b) illustrates the I-V characteristics of the impact of the n^{++} layer under various conditions, specifically the distance (d) between the metals.

The simulation was for a lateral structure where the metal contacts were placed at the left and right top corner with spacing 5, 9, 13, 17, 21, and 25 μm in between the left and right metal contact and n^{++} layer place under the metal contact with the thickness of 54 nm and doping concentration of $1 \times 10^{20} \text{ cm}^{-3}$. The Universal Schottky Tunneling (UST) model was selected to describe the thermionic and field emission processes occurring between a metal contact and heavily doped semiconductor. An effective mass calibration was set for various doping n^{++} layers. Masetti's default mobility model was chosen for this simulation work.

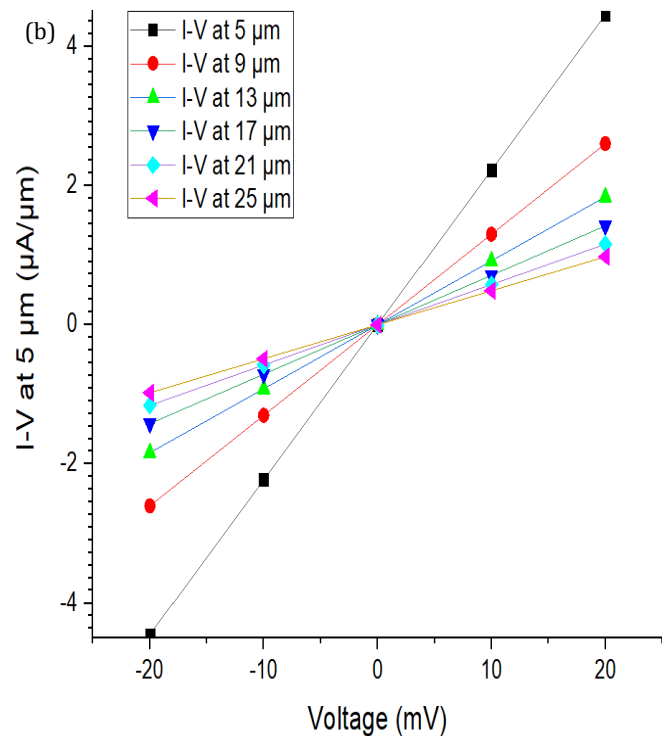
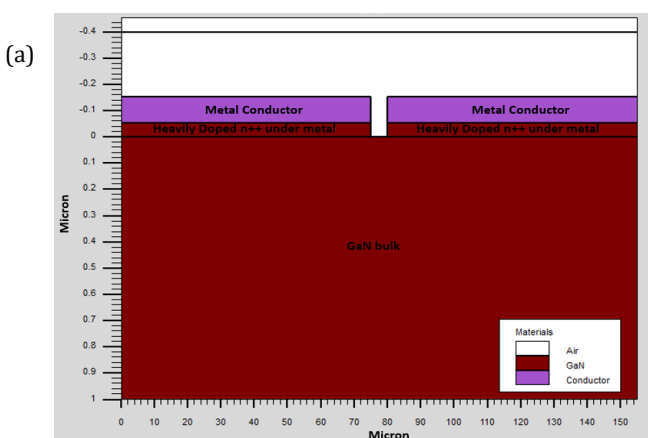


Figure 7. (a) Lateral n-GaN with n^{++} layer under the metal contact. (b) I-V curve of $1 \times 10^{17} \text{ cm}^{-3}$ n-GaN with 54 nm layer thickness of $1e20 \text{ n}^{++}$ under the metal with work-function of $\phi_m=4.3 \text{ eV}$.

In addition, a simulation was also conducted to observe the effect of various n^{++} layer thickness vs. the n^{++} layer doping under the metal that increased from $5 \times 10^{17} \text{ cm}^{-3}$ to $1 \times 10^{20} \text{ cm}^{-3}$; the data are tabulated in Table 4. The decrease in contact resistivity for different doping levels of n^{++} layers nearly approached saturation once the thickness reached 18 nm. Therefore, the heavily doped semiconductor layer plays a crucial role in transferring the contact to ohmic, where the layer is underneath the metal. The existence of this layer can also convert the Schottky contact into an ohmic contact. If the barrier between the metal-semiconductor junction is high, there is an adverse effect where the electron is not able to overcome the barrier height due to insufficient energy; this decreases the thermionic current. However, the existence of a highly doped layer induces electron tunnelling through the junction.

Based on the result of lateral structure, the contact resistivity decreases as per I-V curve showed in Figure 3(c) as per when doping increases hence, further study was conducted to place heavily doped layer n^{++} under the metal to optimize the result of contact resistivity. With the result obtained, the contact resistivity was optimum and started to saturate in 18 nm thickness of heavily doped layer n^{++} with doping of $1 \times 10^{19} \text{ cm}^{-3}$. where the contact resistivity in the magnitude of $10^{-7} \Omega\text{-cm}^2$ versus magnitude of $10^{-6} \Omega\text{-cm}^2$ for the typical metal stack with annealing method. This study imposed the possibility of introducing the non-alloyed type of ohmic contact with strategies of placing the heavily doped n^{++} layer under the metal layer.

Table 3. Lateral n-GaN dimension and specifications.

Metal thickness (nm)	Semiconductor thickness (μm)	Metal contact length (μm)	N doping (cm^{-3})	Spacing between contact (μm)	Metal work function (ϕm)
100	1	75	1×10^{19}	5, 9, 13, 17, 21, 25	4.3

Table 4. Effect of n^{++} layer with different doping and thickness. The doping contact resistivity of n-GaN is $1 \times 10^{17} \text{ cm}^{-3}$.

Doped/Thick (nm)	$5 \times 10^{17} (\text{cm}^{-3})$	$1 \times 10^{18} (\text{cm}^{-3})$	$5 \times 10^{18} (\text{cm}^{-3})$	$1 \times 10^{19} (\text{cm}^{-3})$	$5 \times 10^{19} (\text{cm}^{-3})$	$1 \times 10^{20} (\text{cm}^{-3})$
2	7.988E-05	7.533E-05	4.731E-05	2.551E-05	1.435E-06	1.046E-06
6	5.024E-05	3.389E-05	2.124E-06	1.189E-06	9.497E-07	9.109E-07
18	8.642E-06	2.118E-06	1.082E-06	9.686E-07	9.249E-07	9.018E-07
54	2.451E-06	1.417E-06	9.686E-07	9.018E-07	8.050E-07	7.748E-07

4. CONCLUSION

Introducing a highly doped semiconductor layer has the ability to convert a Schottky contact into an ohmic contact. There is an adverse effect where thermionic current decreases as the energy of electrons is insufficient to overcome the high barrier between the metal-semiconductor surface. A highly doped layer causes electron tunnelling across the junction, which is directly related to the doping level in the layer beneath the metal contact. The non-alloy ohmic contacts were successfully fabricated with a heavily doped Ge ($1 \times 10^{20} \text{ cm}^{-3}$) regrown layer under the metal, and it achieved specific contact resistance in the order of $10^{-6} \sim 10^{-7} \Omega/\text{cm}^2$. A greater doping depth led to a decrease in contact resistivity. Specifically, a doping depth of 10 nm resulted in a precise contact resistance of approximately $10^{-6} \Omega/\text{cm}^2$, whereas a doping depth of 25 nm resulted in a precise contact resistance of around $10^{-7} \Omega/\text{cm}^2$. This demonstrates that utilizing simulation tools to comprehend the physics of the interface in n-GaN devices can aid in comprehending the contacts on p-GaN in future research. Ultimately, this can lead to a decrease in metal contact resistivity and facilitate the production of normally off GaN HEMT transistors.

ACKNOWLEDGMENTS

Authors would like to thank Ministry of Higher Education Malaysia for funding this project via Higher Education Center of Excellence (HiCoE), Institute of Nano Optoelectronics Research and Technology (INOR), with Project Code: A305-KR-AKH002-0000000434-K134, and Research University Incentive (RUI) grant number "1001/PELECT/8014134" under Universiti Sains Malaysia (USM). Thank you also to USM School of Electrical & Electronic Engineering for their support. Moreover, the SILVACO TCAD tool provided by Universiti Teknologi MARA is gratefully acknowledged.

REFERENCES

[1] I.C. Kizilyalli, A.P. Edwards, H. Nie, D. Disney, D. Bour, "High voltage vertical gan p-n diodes with avalanche capability," *IEEE Transactions on Electron Devices*, vol. 60, pp. 3067-3070, 2013.

[2] F. Roccaforte, F. Giannazzo, F. Iucolano, J. Eriksson, M.H. Weng, V. Raineri, "Surface and interface issues in wide band gap semiconductor electronics," *Applied Surface Science*, vol. 256, pp. 5727-5735, 2010.

[3] E. Gurpinar, F. Iannuzzo, Y. Yang, A. Castellazzi, F. Blaabjerg, "Design of low-inductance switching power cell for GaN HEMT based inverter," *IEEE Transactions on Industry Applications*, vol. 54, pp. 1592-1601, 2018.

[4] M. Kuzuhara and H. Tokuda, "Low-loss and high-voltage III-nitride transistors for power switching applications," *IEEE Transactions on Electron Devices*, vol. 62, pp. 405-413, 2015.

[5] K.J. Chen, O. Haberlen, A. Lidow, C.I. Tsai, T. Ueda, Y. Uemoto, and Y. Wu, "GaN-on-Si power technology: devices and applications," *IEEE Transactions on Electron Devices*, vol. 64, pp. 779-795, 2017.

[6] Z. Wang, L. Li, and Y. Yao, "A Machine Learning-Assisted Model for GaN Ohmic Contacts Regarding the Fabrication Processes," *IEEE Transactions on Electron Devices*, vol. 68, pp. 2212-2219, 2021.

[7] E. Gurpinar and A. Castellazzi, "Single-phase T-type inverter performance benchmark using Si IGBTs, SiC MOSFETs and GaN HEMTs," *IEEE Transactions on Power Electronics*, vol. 31, no. 10, pp. 7148-7160, 2016.

[8] E. A. Jones, F. F. Wang, and D. Costinett, "Review of commercial GaN power devices and GaN-based converter design challenges," *IEEE Journal of Emerging and Selected Topics in Power Electronics*, vol. 4, pp. 707-719, 2016.

[9] T. P. Chow and R. Tyagi, "Wide bandgap compound semiconductors for superior high-voltage unipolar power devices," *IEEE Transactions on Electron Devices*, vol. 41, no. 8, pp. 1481-1483, 1994.

[10] U. K. Mishra, P. Parikh, and Yi-Feng Wu, "AlGaIn/GaN HEMTs - an overview of device operation and applications," *Proceedings of the IEEE*, vol. 90, no. 6, pp. 1022-1031, 2002.

[11] Z. Fan, S.N. Mohammad, W. Kim, Ö. Aktas, A.E. Botchkarev, and H. Morkoç, "Very low resistance multilayer Ohmic contact to n-GaN," *Applied Physics Letters*, vol. 68, pp. 1672-1674, 1996.

- [12] Q. Feng, L.-M. Li, Y. Hao, J.-Y. Ni, and J.-C. Zhang, "The improvement of ohmic contact of Ti/Al/Ni/Au to AlGa_N/Ga_N HEMT by multi-step annealing method," *Solid-State Electronics*, vol. 53, pp. 955-958, 2009.
- [13] Y.-L. Lan, H.-C. Lin, H.-H. Liu, G.-Y. Lee, F. Ren, S.J. Pearton, M.-N. Chang, and J.-I. Chyi, "Low-resistance smooth-surface Ti/Al/Cr/Mo/Au n-type Ohmic contact to AlGa_N/Ga_N heterostructures," *Applied Physics Letters*, vol. 94, no. 24, p. 243502, 2009.
- [14] J.-G. Lee, H.-S. Kim, D.-H. Kim, S.-W. Han, K.-S. Seo, and H.-Y. Cha, "Au-free AlGa_N/Ga_N heterostructure field-effect transistor with recessed overhang ohmic contacts using a Ti/Al bilayer," *Semiconductor Science and Technology*, vol. 30, no. 8, 2015.
- [15] M.O. Yusuke Takei, Wataru Saito, Kazuo Tsutsui, Kuniyuki Kakushima, Hitoshi Wakabayashi, Yoshinori Kataoka and Hiroshi Iwai, "Ohmic contact properties depending on AlGa_N layer thickness for AlGa_N/Ga_N high electron mobility transistor structures," *ECS Transactions*, vol. 61, no. 4, p. 265, 2014.
- [16] G. Greco, F. Iucolano, and F. Roccaforte, "Ohmic contacts to Gallium Nitride materials," *Applied Surface Science*, vol. 383, pp. 324-345, 2016.
- [17] C. Huh, S.-W. Kim, H.-S. Kim, I.-H. Lee, and S.-J. Park, "Effective sulfur passivation of an n-type Ga_N surface by an alcohol-based sulfide solution," *Journal of Applied Physics*, vol. 87, no. 9, pp. 4591-4593, 2000.
- [18] F. Iucolano, G. Greco, and F. Roccaforte, "Correlation between microstructure and temperature dependent electrical behavior of annealed Ti/Al/Ni/Au Ohmic contacts to AlGa_N/Ga_N heterostructures," *Applied Physics Letters*, vol. 103, no. 20, 2013.
- [19] C. Wang and N.Y. Kim, "Electrical characterization and nanoscale surface morphology of optimized Ti/Al/Ta/Au ohmic contact for AlGa_N/Ga_N HEMT," *Nanoscale Research Letters*, vol. 7, no.107, 2012.
- [20] L. Wang, F.M. Mohammed, and I. Adesida, "Differences in the reaction kinetics and contact formation mechanisms of annealed Ti / Al / Mo / Au Ohmic contacts on n-Ga_N and AlGa_N / Ga_N epilayers," *Journal of Applied Physics*, vol. 101, no. 1, 2007.
- [21] J. S. Foresi and T. D. Moustakas, "Metal contacts to gallium nitride," *Applied Physics Letters*, vol. 62, no. 22, pp. 2859-2861, 1993.
- [22] M. E. Lin, Z. Ma, F. Y. Huang, Z. F. Fan, L. H. Allen, and H. Morkoç, "Low resistance ohmic contacts on wide band-gap Ga_N," *Applied Physics Letters*, vol. 64, no. 8, pp. 1003–1005, 1994.
- [23] Y.-F. Wu, W.-N. Jiang, B.P. Keller, S. Keller, D. Kapolnek, S.P. Denbaars, U.K. Mishra, and B. Wilson, "Low resistance ohmic contact to n-Ga_N with a separate layer method," *Solid-State Electronics*, vol. 41, no. 2, pp. 165-168, 1997.
- [24] Y.-L. Lan, H.-C. Lin, H.-H. Liu, G.-Y. Lee, F. Ren, S.J. Pearton, M.-N. Chang, and J.-I. Chyi, "Low-resistance smooth-surface Ti/Al/Cr/Mo/Au n-type ohmic contact to AlGa_N/Ga_N heterostructures," *Applied Physics Letters*, vol. 94, no. 24, pp. 243502, 2009.
- [25] A.-J. Tzou, D.-H. Hsieh, S.-H. Chen, Z.-Y. Li, C.-Y. Chang, H.-C. Kuo, "Non-thermal alloyed ohmic contact process of Ga_N-based HEMTs by pulsed laser annealing," *Semiconductor Science and Technology*, vol. 31, 2016.
- [26] A.V. Zhelannov and B.I. Seleznev, "Non-alloyed ohmic Cr/Pt/Au contacts to Ga_N based structures," *IOP Conference Series: Materials Science and Engineering*, vol. 441, 2018.
- [27] D.K. Schroder, *Semiconductor Material and Device Characterization*, Third Edition, 2006.
- [28] C. Sharma, A. K. Visvkarma, R. Laishram, A. Kumar, D. S. Rawal, S. Vinayak, and R. Singh, "Effect of γ -ray irradiation on Schottky and ohmic contacts on AlGa_N/Ga_N hetero-structures," *Microelectronics Reliability*, vol. 105, p. 113565, 2020.
- [29] D.A. Neamen, *Semiconductor Physics and Devices: Basic Principles*, McGraw-Hill, 2012.